Waste Management 81 (2018) 1–10

Contents lists available at ScienceDirect

Waste Management

journal homepage: www.elsevier.com/locate/wasman

Leaching behaviour of co-disposed steel making wastes: Effects of aeration on leachate chemistry and vanadium mobilisation

Andrew J. Hobson [a], Douglas I. Stewart [b], Robert J.G. Mortimer [c], William M. Mayes [d], Mike Rogerson [d], Ian T. Burke [a,*]

[a] School of Earth and Environment, University of Leeds, Leeds LS2 9JT, UK
[b] School of Civil Engineering, University of Leeds, Leeds LS2 9JT, UK
[c] School of Animal, Rural and Environmental Sciences, Nottingham Trent University, Brackenhurst Campus, Southwell, Nottinghamshire NG25 0QF, UK
[d] School of Environmental Sciences, University of Hull, Hull HU6 7RX, UK

ARTICLE INFO

Article history:
Received 24 April 2018
Revised 24 August 2018
Accepted 28 September 2018

Keywords:
Steel slag
Vanadium
Leaching behaviour
Alkaline wastes

ABSTRACT

Steelmaking wastes stored in landfill, such as slag and spent refractory liners, are often enriched in toxic trace metals (including V). These may become mobile in highly alkaline leachate generated during weathering. Fresh steelmaking waste was characterised using XRD, XRF, and SEM-EDX. Batch leaching tests were performed under aerated, air-excluded and acidified conditions to determine the impact of atmospheric CO_2 and acid addition on leachate chemistry. Phases commonly associated with slag including dicalcium silicate, dicalcium aluminoferrite, a wüstite-like solid solution and free lime were identified, as well as a second group of phases including periclase, corundum and graphite which are representative of refractory liners. During air-excluded leaching, dissolution of free lime and dicalcium silicate results in a high pH, high Ca leachate in which the V concentration is low due to the constraint imposed by $Ca_3(VO_4)_2$ solubility limits. Under aerated conditions, carbonation lowers the leachate pH and provides a sink for aqueous Ca, allowing higher concentrations of V to accumulate. Below pH 10, leachate is dominated by periclase dissolution and secondary phases including monohydrocalcite and dolomite are precipitated. Storage of waste under saturated conditions that exclude atmospheric CO_2 would therefore provide the optimal environment to minimise V leaching during weathering.

1. Introduction

Steel slag is a ubiquitous byproduct of the steelmaking industry that is produced in large quantities worldwide. It is estimated that 160–240 million tonnes of steel slag were produced in 2016 (Ober, 2017) which corresponds to approximately 10–15% of crude steel output (Piatak et al., 2014). Primary steelmaking (i.e. conversion of iron to steel) produces steel slag via two principal production methods; (1) basic oxygen furnace (BOF) steelmaking in which molten iron from a blast furnace is used and (2) electric arc furnace (EAF) steelmaking which uses a combination of scrap steel, directly reduced iron and pig iron. In both processes lime (or limestone) is added to the furnace as a fluxing agent to remove impurities from the molten metal (Eloneva et al., 2010; Piatak et al., 2014). The composition of BOF and EAF slag is broadly similar and consistent across location and process (Tossavainen et al., 2007; Yildirim and Prezzi, 2011; Proctor et al., 2000). These predominantly consist of Ca, Mg, Fe and Al oxides and silicates (Proctor et al., 2000); the relative proportions of which will vary according to the raw materials used during manufacture. Secondary steelmaking slags are formed during secondary steelmaking where both BOF and EAF derived steels are further processed in ladle furnaces, producing BOF(L) or EAF(L) slags respectively. These are much more variable in composition and are also relatively enriched in Mg and Al due to additives used in the process (Shi, 2002). In addition to slag production, a wide variety of refractories (MgO-C; Al-silicate; MgO-Al_2O_3-C) are used as furnace liners during steelmaking to protect the furnace (Quaranta et al., 2014). Refractories that are in contact with molten slag wear over time and the build-up of solidified slag above the melt (due to sputtering) and in conduits also require regular removal. Therefore, periodic renewal of the entire liner is required. The result is a mixed waste containing both slag and refractories which is difficult to separate and are often co-disposed (Hanagiri et al., 2008).

Primary steelmaking slags are recycled where possible, usually as aggregate in civil engineering applications, such as road construction and as a general fill material due to its stability (Geiseler, 1996;

* Corresponding author.
E-mail address: i.t.burke@leeds.ac.uk (I.T. Burke).

https://doi.org/10.1016/j.wasman.2018.09.046
0956-053X/

Yi et al., 2012). However, in some cases elevated concentrations of free lime (CaO) and periclase (MgO), which expand on hydration, preclude reuse in engineering applications. Ladle slags and refractories can also be recycled during primary steelmaking (as an alternative source of CaO or MgO flux) but virgin materials are often preferred due to their more uniform composition and the increased effort that would be required in slag sorting and processing (Kwong and Bennett, 2002; de Sa et al., 2007). For this reason, and also because supply frequently exceeds the demand for secondary aggregates, steelmaking byproducts are often stored either in landfill or in open 'heaps'. However, as recycling rates increase, materials with problematic properties (e.g. high metal content, high % of CaO or MgO, or simply uncertain or variable composition) will make up an ever greater proportion of materials stored in landfill. It is therefore increasingly import to understand the leaching behaviour of such non-standard by-products as they become a significant part of the disposed inventory.

Steel slags contain free lime (CaO) and periclase (MgO; also in present in refractories) that hydrate to form portlandite ($Ca(OH)_2$) or brucite ($Mg(OH)_2$). These phases dissolve in water to generate high pH (10.5–12.5) leachate (Mayes et al., 2008):

$$CaO_{(s)} + H_2O \rightarrow Ca(OH)_{2(aq)} \rightleftharpoons Ca^{2+} + 2OH^- \quad pH_{(eq.)} = 12.46 \tag{1}$$

$$MgO + H_2O \rightarrow Mg(OH)_{2(aq)} \rightleftharpoons Mg^{2+} + 2OH^- \quad pH_{(eq.)} = 10.40 \tag{2}$$

Alkalinity may also be produced by the dissolution of Ca-silicates, (e.g. β-dicalcium silicate, larnite; Roadcap et al. (2005)):

$$Ca_2SiO_4 + 2H_2O \rightarrow 2Ca^{2+} + H_2SiO_4{}^{2-} + 2OH^- \tag{3}$$

In addition, under aerated conditions, reactions involving the in-gassing of CO_2 results in conversion of Ca/Mg hydroxide based alkalinity to carbonate alkalinity.

$$Ca^{2+}{}_{(aq)} + CO_{2(aq)} + 2OH^-{}_{(aq)} \rightarrow CaCO_{3(s)} + H_2O_{(l)} \tag{4}$$

$$CaCO_3 + H_2O \rightleftharpoons Ca^{2+} + HCO_3{}^- + OH^- \quad pH_{(eq.)} = 9.36 \tag{5}$$

Whilst steel slag has historically been considered to be a non-hazardous waste, concerns have been raised in recent years regarding the high concentrations of potential toxic trace metal(loid)s (including Al, Cr, Pb, Mo and V) present in the slag (Tossavainen et al., 2007; Proctor et al., 2000; Matern et al., 2013) which may be mobilised in the alkaline leachate (Cornelis et al., 2008). V leaching in particular has received a lot of recent attention (Chaurand et al., 2006; De Windt et al., 2011; Huijgen and Comans, 2006; Navarro et al., 2010) due to its relative enrichment in steel slags and regulatory concern over high V concentrations in leachates (Environment Agency, 2014). Steelmaking wastes at disposal sites are often deposited in both saturated and unsaturated settings, however, few data currently exist concerning slag leachate generation and chemistry under aerated conditions (Bayless and Schulz, 2003; Roadcap et al., 2005; Mayes and Younger, 2006). Under aerated conditions, $CaCO_3$ precipitation results in a drop in solution pH as OH^- ions are consumed (Eq. (4)). Changes in both pH and redox have significant implications for the mobility of many potentially toxic metals; for example Al, Cr, and V mobility and toxicity are all highly dependent on their speciation (with higher oxidation states generally regarded as more toxic and mobile) (Pourbaix, 1966).

This study investigates leaching behaviour of co-disposed steelmaking waste under aerated and air-excluded conditions. These represent contrasting conditions present either near the surface (good contact with atmosphere) and below the water table deeper within waste heaps. The waste has been characterised using X-ray diffraction (XRD) and fluorescence (XRF) techniques, as well as scanning electron microscopy (SEM) with energy-dispersive X-ray spectroscopy (EDX) to determine the mineral phases present. Fully aerated and air-excluded water leaching tests have been performed to determine how phase dissolution behaviour, secondary mineral formation and trace metal release are affected by changes in pH and availability of air. Results will assist prediction of metal release from waste when stored in landfill above and below the water table, enabling effective environmental risk assessment and cost-effective long-term management of the waste.

2. Methods and materials

2.1. Sample collection and characterisation

Samples were collected within one week of deposition from the Yarborough Landfill (British Steel, Scunthorpe, UK) in May 2013 (LAT 53°35′22.24″ LONG 0°35′41.52″). The sample consisted of 50–500 g blocks (~100 kg total). A sub-sample of the collected material (approx. 500 g consisting of 50 g pieces) were brushed to remove any fines and crushed to provide a homogenised powder consisting of 20–100 μm particles. The crushed waste was stored in a polythene bag within an airtight glass jar containing soda lime to prevent weathering due to contact with atmospheric CO_2 and moisture.

Elemental analysis of the powdered waste was undertaken using a PANalytical Axios Advanced X-ray Fluorescence (XRF) spectrometer (data corrected for loss on ignition at 1050 °C). Samples were prepared for major element analysis as fused beads with lithium metaborate/tetraborate flux (Johnson Matthey Spectroflux JM100B) (0.6 g sample; 3 g flux). For minor/trace element analysis pressed pellets were prepared containing ~10 g of dried waste using ~10–20 drops of 6.6% w/v polyvinyl alcohol in a 1:6 mix of methanol and distilled deionized water as a binder (Moviol 88 solution). The elemental limit of detection (LoD) was generally <0.02 wt% and the analytical uncertainty (versus certified reference standards) was <±10% of the data value. Mineralogical analysis (LoD was approximately 3 wt% for crystalline phases) was undertaken by powder X-ray diffraction (XRD) using a Bruker D8 diffractometer, where powder samples were mounted on silicon slides and scanned between 2° and 70° 2θ using Cu K_α radiation. Diffraction peaks from unknown samples were then matched to known standard reference patterns using Diffrac.Suite Eva v3.0 software using the International Centre for Diffraction Data (ICDD) PDF2 database (powder diffraction file (PDF) reference numbers are reported for identified phases).

Two polished blocks were prepared by first cutting waste pieces to size under water and setting the resultant ~2 cm^3 blocks into epoxy resin with the cut surface exposed. This surface was then polished using a water-free diamond paste to remove the top 1–2 mm of material potentially exposed to water during cutting. Electron micrographs were subsequently collected on a FEI QUANTA 650 FEG ESEM, which was equipped for Oxford Instruments INCA 350 energy-dispersive X-ray spectroscopy (EDS) system/80 mm X-Max silicon drift detector. EDS spectra and elemental maps were collected and analysed using Oxford Instruments AZtec software. The element and sample specific LoD for EDS analysis was between 0.1 and 0.5 wt%.

2.2. Acid neutralisation capacity (ANC)

Homogenised powdered waste (0.4 g) was mixed with 40 mL HCl with concentrations ranging from 1 M to 0.001 M in 50 mL polypropylene Oak Ridge tubes (Nalgene, USA). Experiments were performed in triplicate. Headspaces of the 50 mL tubes were

flushed with N_2 gas prior to sealing. All tubes were subsequently stored in airtight 2 L glass jars (Le Parfait, France) filled with N_2 gas and also containing ~100 g soda lime (as a CO_2 absorbent) to prevent any CO_2 infiltration from atmosphere to the experimental tubes. After 1 and 50 days equilibration the 50 mL tubes were centrifuged in a Sigma 2–16 centrifuge using a 12,151 rotor at 8000 rpm (6000*g*) for 5 min to separate aqueous and solid phases. 1 mL of the supernatant was removed and immediately added to 9 mL 0.1 M HNO_3 prior to ICP analysis, and the pH of the remaining solution was measured (pH measurement is described below).

2.3. Leaching tests

Triplicate aerated experiments containing 1 g homogenised powdered waste and 100 mL deionised water were established in open 500 mL PETG Erlenmeyer flasks. These were gently agitated on a Stuart Scientific SSL1 orbital shaker at 175 rpm to allow for equilibrium of the reaction solution with air (i.e. dissolution of atmospheric CO_2 and O_2). At regular intervals over a 50 day period 3 mL aliquots of slurry were removed from the flasks and centrifuged in 2 × 1.5 mL Eppendorf tubes in a Spectrafuge 16 M microcentrifuge at 14,000 rpm (16,000*g*) for 5 min to separate aqueous and solid phases. 1 mL of supernatant was removed and acidified in 0.1 M HNO_3 and the pH of the remaining supernatant was determined. The moist solid samples were stored at −20 °C prior to drying at 40 °C overnight for further analysis.

Replicate air-excluded experiments were established containing 0.4 g homogenised powdered waste and 40 mL deionised water in 50 mL Oak ridge tubes. All tubes were anaerobically handled as described above for the ANC tests. Periodically over a 50 day period 3 tubes were sacrificially sampled. Solid and solution samples were taken and stored following the procedures above.

2.4. Aqueous analysis

Solution pH (±0.2 pH units) was measured using an Orion DualStar pH/ISE benchtop meter (Thermo Scientific, USA) with an electrode that was calibrated daily at pH 4, 7 and 10. Nitrogen gas was bubbled through the sample tube during pH measurements made in solutions from the air-excluded experiments to prevent contact with atmosphere. Metal concentrations in acidified aqueous samples from the air-excluded leaching experiments were determined (with an analytical uncertainty of <±3%) using a Thermo iCAP 7400 ICP-OES ion-coupled plasma, optical emission spectrometer (ICP-OES; for Ca, Si, Mg; LoDs were <10 μg L^{-1}) and Thermo iCAP Qc ion-coupled plasma, mass spectrometer (ICP-MS; for V, Mn, and Cr with LoDs <0.1 μg L^{-1}; for Li and Fe with LoD <2 μg L^{-1}). Calibration was against certified multi-element standards and check samples were analysed every 10 samples to check for calibration drift. Aqueous elemental concentrations from the aerated leaching experiments were determined using a Perkin Elmer Optima 5300DV ICP-OES for all elements (LoDs were <100 μg L^{-1} for all elements). The 5300DV was calibrated with 3 standards (0.1, 1, 10 mg L^{-1}) and a blank which were run every 15 samples and the calibration cross-checked with a trace metal Certified Reference Material (NIST1646A) with all values within ±5%.

3. Results

3.1. Material characterisation

The elemental composition (Table 1) of the powder sample was dominated by Ca, Fe, Mg, Si and Al with Cr and Mn as minor constituents. Trace elements included P, V, K, Ti and S.

Table 1
Chemical composition of BOF steel slag samples from the Yarbrough Repository, Scunthorpe UK, and the powder sample used in leaching tests.

Major Elements Nominal Oxide wt%	BOF slag (Hobson et al., 2017)	Powder sample (this study)
CaO	40 ± 5	19 ± 2
FeO	32 ± 9	16 ± 2
SiO_2	14 ± 3	11 ± 1
MgO	5.2 ± 1	28 ± 3
MnO	4.5 ± 1	2.1 ± 0.2
Al_2O_3	1.2 ± 0.4	18 ± 2
P_2O_5	1.3 ± 0.4	0.87 ± 0.09
V_2O_5	0.81 ± 0.24	0.33 ± 0.03
TiO_2	0.30 ± 0.13	0.86 ± 0.09
Cr_2O_3	0.24 ± 0.13	3.3 ± 0.3
SO_3	0.23 ± 0.09	0.33 ± 0.03
K_2O	n.d.	0.12 ± 0.01
Na_2O	n.d.	0.18 ± 0.02
SrO	n.d.	0.14 ± 0.01
ZrO_2	0.02 ± 0.01	0.14 ± 0.01
BaO	n.d.	0.01 ± 0.01
NiO	0.02 ± 0.01	n.d.
CuO	0.01 ± 0.01	n.d.
ZnO	n.d.	0.02 ± 0.01
PbO	n.d.	0.03 ± 0.01
LOI	*n.d.*	*0.96*
TOTAL	98.9	100.9

Mineralogical analysis of the crushed waste using XRD (Fig. 1a) identified the presence of periclase (MgO; PDF #44-946), corundum (Al_2O_3; PDF #10-173), larnite (dicalcium silicate, β-Ca_2SiO_4; PDF #33-302), brownmillerite (dicalcium aluminoferrite, $Ca_2(Al,Fe)_2O_5$; PDF #30-226), wüstite (FeO; PDF #46-1312), brucite ($Mg(OH)_2$; PDF #44-1482) and elemental carbon (graphite-C; PDF #23-64). The principal XRD peak of free lime (CaO; PDF #37-1497) overlaps with a secondary peak of corundum at ~37.5° 2θ, however, the secondary peaks at ~32 and 54° 2θ were present, suggesting its presence. There was no calcite peaks in the XRD pattern for the unreacted waste (n.b. the principle calcite peak is at ~29° 2θ).

SEM analysis of a polished block (Fig. 2) showed a material that was composed of intergrown 10–30 μm crystallites, EDS elemental mapping indicated that there were three dominant compositions. The dominant composition by area (~65% of the sample viewed) was a Ca-Si-O rich phase containing trace amounts of Al, P, Ti, V and Fe by EDS analysis, consistent with the larnite phase identified by XRD. The second most abundant composition by area (~25%) was a Mg-Fe-O rich phase containing trace amounts of Na, Ca, Cr and Mn, corresponding to the wüstite phase identified by XRD. The third most abundant composition by area (~10%) was a Ca-Fe-Al-O rich phase containing trace amounts of Ti, V, Cr and Mn, corresponding to the brownmillerite phase identified by XRD. Regions of the dicalcium silicate phase contain lamellae identified as CaO rich regions associated with dicalcium silicate. The second polished block was composed of a single Al-Si-O rich composition containing no significant trace elements (data not shown).

3.2. Acid neutralisation tests

For crushed waste, the relationship between the final solution pH value and the amount of acid added was similar after 1 day and 50 days of equilibration (Fig. 3a). The acid neutralisation capacity (to pH 7) was very similar at the two time-points (11.0 and 9.5 M H^+ kg^{-1} waste, respectively). In tests where the final pH value was >7, the pH value increased with time. The solution Ca and Mg concentrations at a particular pH value were broadly similar after 1 day and 50 days (Fig. 3c, d), however, Si (Fig. 3b) was present in solution at all final pH values <10 after 1 day, but

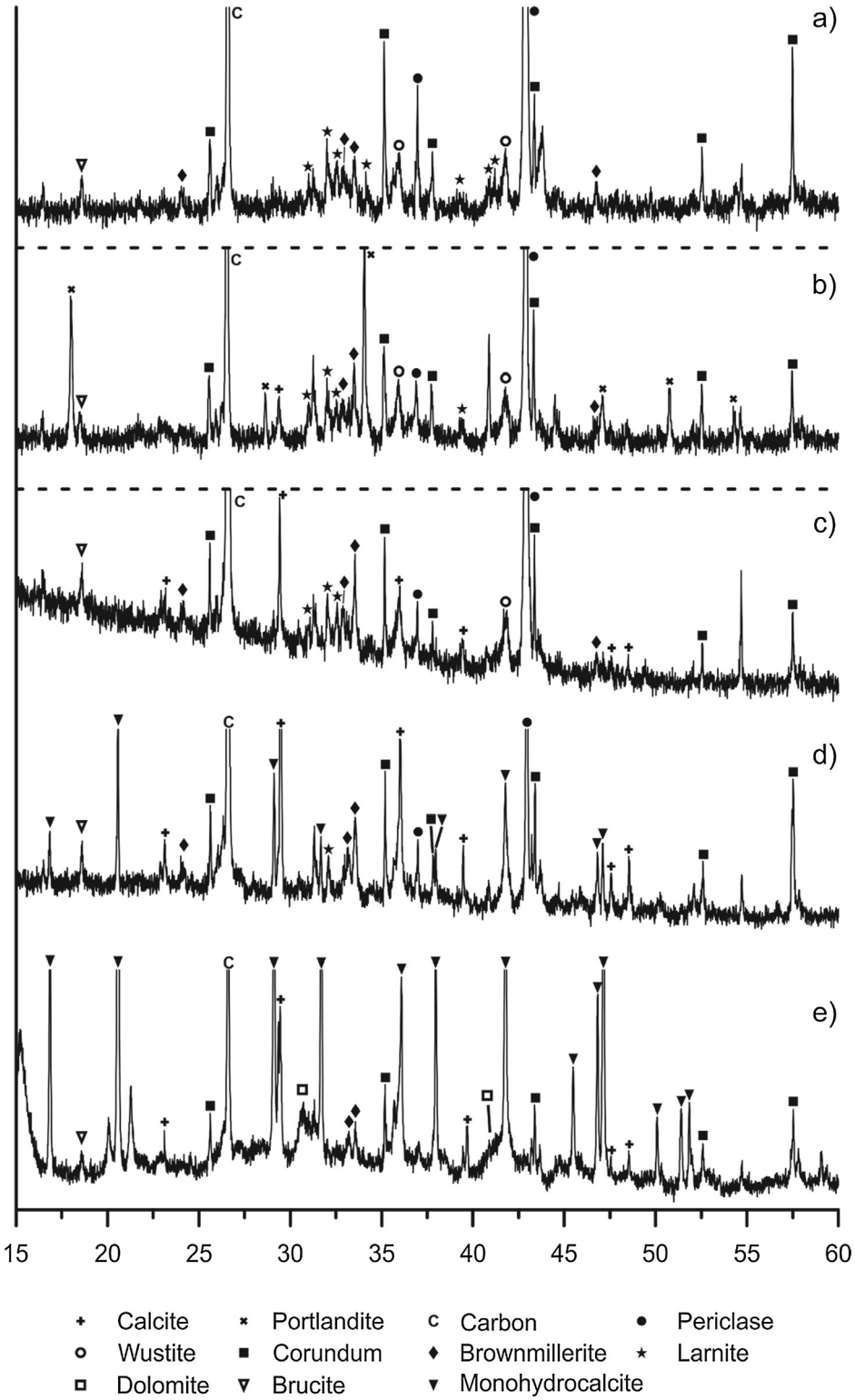

Fig. 1. XRD patterns from (a) unweathered steelmaking waste, (b) steelmaking waste leached for 50 days under air-excluded conditions, and steelmaking waste leached under aerated conditions for (c) 1 h, (d) 6 days and (e) 50 days.

was present at significantly reduced concentrations at 50 days at all pH values. Calcium was released to solution at all pH values, with generally higher concentrations at lower pH values. Magnesium was only present in solution below ~pH 10, but also has generally higher concentrations at lower pH values.

3.3. Batch leaching tests

During air-excluded leaching (Fig. 4), the leachate pH rose rapidly within the first hour to a value of 11.4, and then increased more slowly to a maximum value of 11.9 after 52 days. The Ca

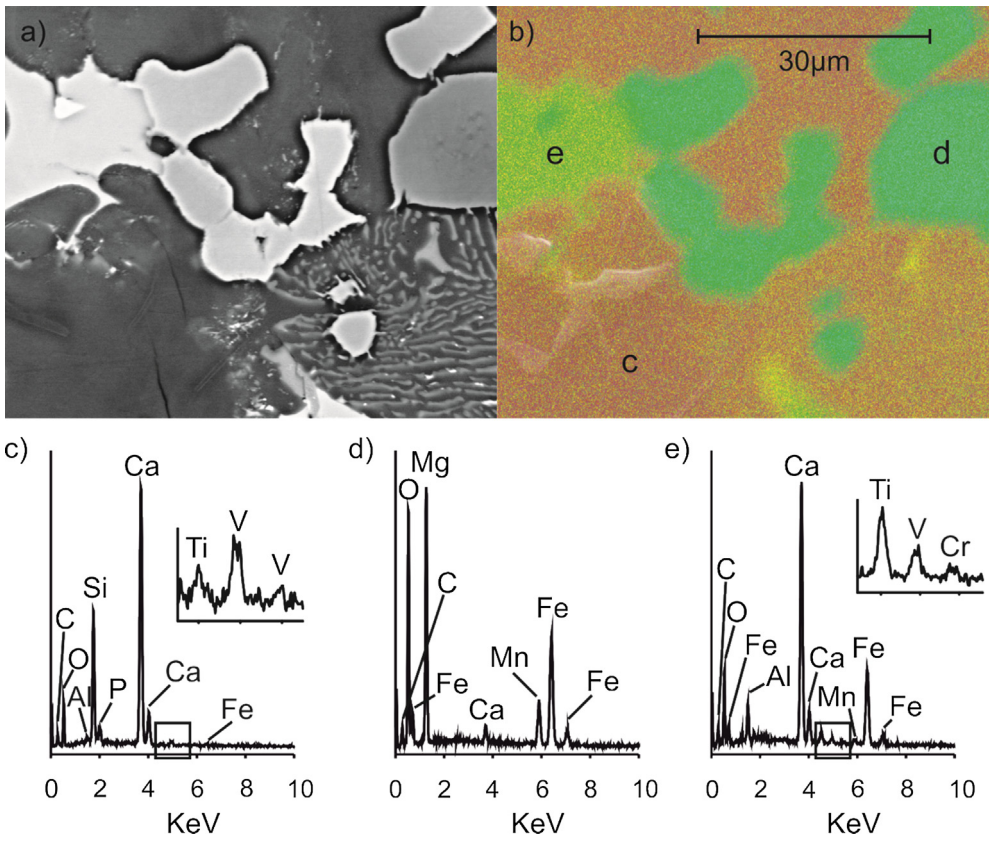

Fig. 2. Backscattered electron micrograph (top left) with corresponding false colour element map (top right) and EDS spectra from (c) dicalcium silicate, (d) wüsite and (e) dicalcium aluminoferrite phases. The laminae containing phase (bottom right) also contains discrete CaO laminae.

concentration increased rapidly to ~2.5 mmol L^{-1} over the first 24 h, and then more steadily to ~3.0 mmol L^{-1} after 5 days. Between 5 days and 10 days the Ca concentration decreased to ~2.5 mmol L^{-1}, but thereafter increased steadily to ~3.4 mmol L^{-1} after 50 days. The Mg concentration showed no trend with time and was <0.4 mmol L^{-1} throughout the experiment. The Si concentration increased to ~0.15 mmol L^{-1} over the first 24 h, and then to ~0.25 mmol L^{-1} after 5 days. After about 10 days the Si concentration decreased to ~0.15 mmol L^{-1} but subsequently varied between ~0.15 and ~0.25 mmol L^{-1} until the end of the test. The V concentration gradually increased from ~0.002 mmol L^{-1} after 24 h to ~0.007 mmol L^{-1} after 50 days. Aqueous Fe concentrations range from 0.002 to 0.07 mmol L^{-1} and were just above the limit of detection by ICP-MS (0.0018 mmol L^{-1}), which increases scatter in the data. However, it is still discernible that Fe accumulated in solution during the air-excluded experiments and did not in parallel aerated experiments. There was very little change in XRD patterns collected from the solid residue over time, except that portlandite (PDF #44-1481) was detected in samples collected from the experiment end points (Fig. 1b).

During the aerated experiments (Fig. 4), pH increased rapidly within the first hour to a maximum value of 11.6. This was followed by a decrease to pH 8.9 after 1 day and then by a second rise to pH 10.0 after 6 days. Subsequently pH steadily declined to 9.3 after 50 days of leaching. The Ca concentration increased rapidly to ~2 mmol L^{-1} within the first two hours, but then decreased to ~0.25 mmol L^{-1} after 6–7 days. Initially the Mg concentration was low but it increased rapidly after day 2 to reach a concentration above 12.5 mmol L^{-1} by day 20, which persisted until the end of the test. The Si concentration was ~0.15 mmol L^{-1} after 1 h, decreased to ~0.03 mmol L^{-1} after 2 days but then rose to ~0.25 mmol L^{-1} at 6 days. Subsequently Si concentrations remained above 0.2 mmol L^{-1} for the remainder of the test. The V concentration increased steadily over the duration of the test to reach a maximum of ~0.065 mmol L^{-1} after 48 days. The aqueous Fe concentrations were initially around 0.05 mmol L^{-1} and decreased over 5 days to <0.002 mmol L^{-1} for the remainder of the tests. XRD patterns collected from solid residue after 1 day show that calcite (PDF #24-27) was present (Fig. 1c), after 6 days the periclase and larnite peaks had reduced in relative intensity and monohydrocalcite (PDF #29-306) was detected (Fig. 1d). After 50 days monohydrocalcite was the dominant secondary phase detected (although some dolomite, PDF #36-426, was also present) and periclase and larnite peaks were absent (Fig. 1e).

Concentrations of other trace elements considered to be potential environmental risk drivers for steel slags (e.g. Mn, Cr, Li) were low in both the aerated and the air-excluded tests (and were present at concentrations close to or below to the limit of detection).

4. Discussion

4.1. Waste characterisation

The bulk chemical and mineralogical composition of the waste was distinct from BOF slag samples collected at the Yarborough site (Table 1). Compared to BOF slag the material was relatively depleted in elements such as Ca, Fe, Mn and V; but enriched in Mg, Al, Ti and Cr. The waste mineralogy could be split into two distinct groups. The first group included a range of phases commonly occurring in BOF slag (i.e. larnite, brownmillerite, lime, and wüstite; Yildirim and Prezzi, 2011; Proctor et al., 2000; Geiseler, 1996), which were observed in SEM as discrete particle assemblages within an intergrown matrix of 20–50 μm crystallites. The

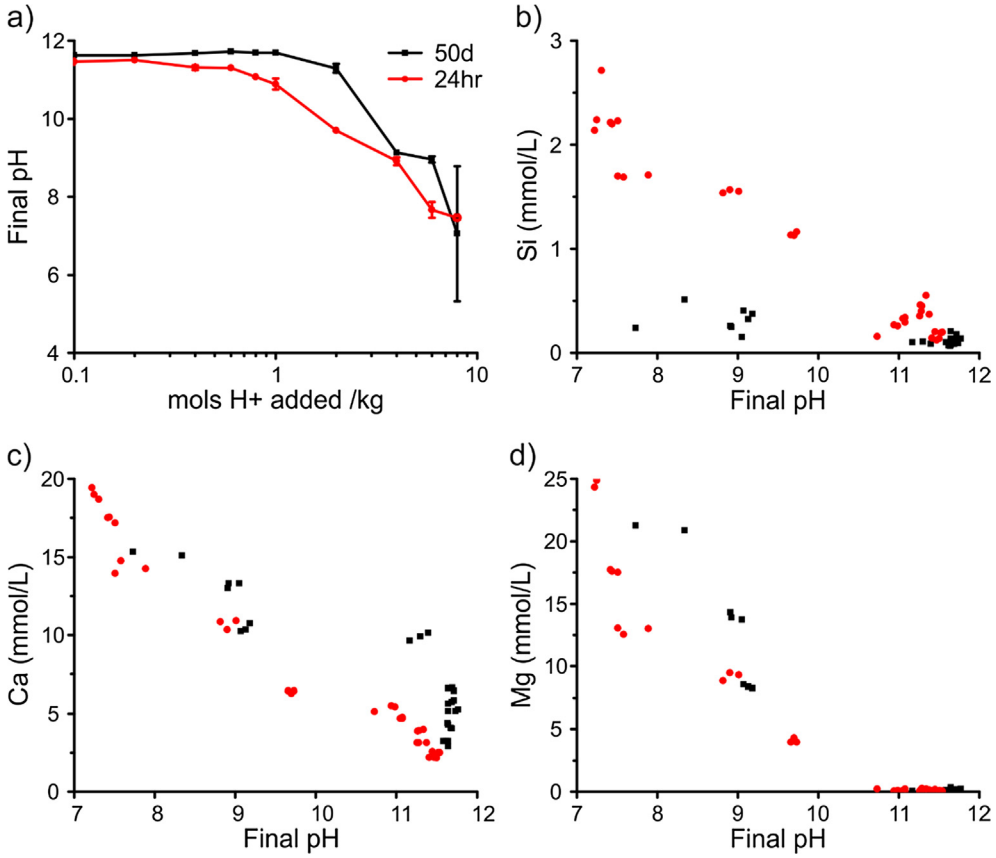

Fig. 3. Acid neutralisation results showing (a) final pH values after 24 h (red circles) and 50 days (black squares) as a function of initial acid concentration (each point represents the mean value and error bars ±1σ from triplicate samples) and (b–d) metal concentrations leached from waste over 24 h and 50 days as a function of final pH. Initial test conditions in all cases were 10 g waste L^{-1}. (For interpretation of the references to colour in this figure legend, the reader is referred to the web version of this article.)

second group of minerals identified by XRD included corundum, periclase and graphite that are rare in BOF slag and are more commonly associated with refractory liner materials (e.g. in MgO-C and AL_2O_3-MgO-C refractories; Rovnushkin et al., 2005). Aluminosillicate was also observed in SEM analysis. This was most likely the high temperature phase mullite ($Al_6Si_2O_{13}$; Schneider et al., 1994; Chesters, 1973; Mazdiyasni and Brown, 1972; Tamari et al., 1993) which is also used as a refractory material or can form in slags from reaction of corundum and Si (Dana and Das, 2004; Zhao et al., 2014). Therefore, the waste can be characterised as a mixed steelmaking waste containing both BOF slag and refractory materials. The potential for re-use of mixed wastes is low due to uncertainties about their chemical and physical behaviour, however, it is important to understand their potential leaching behaviour during disposal.

4.2. Acid neutralisation behaviour

The acid neutralisation capacity experiments were conducted under air-excluded conditions and provide information on phase dissolution in the waste as a function of the acid addition and final solution pH. At low acid additions (<1 mol H^+ kg^{-1}) the waste buffered pH to values >11.5 due to the dissolution of free lime and dicalcium silicate (Eqs. (1) and (3)), with dissolution of brucite from periclase hydration also consuming acid when the pH < 10.4 (Eq. (2)). Ca was released to solution at all pH values with the amount of release increasing with decreasing pH (Fig. 3c), and Mg was released to solution when pH values <10 with the amount of release also increasing with decreasing pH (Fig. 3d), which is consistent with the dissolution behaviour of these phases (Eqs. (1) and (2)). The alkalinity producing phases were progressively exhausted by larger acid additions and the final pH decreased steadily until neutral values were reached with an acid addition of ~8 mols H^+ kg^{-1}. CaO hydration is a very fast reaction (Shi et al., 2002), whereas dicalcium silicate hydration and dissolution is generally considered to be slower (Taylor, 1986). However, here we find that both are involved in buffering the pH in the first 24 h as Si is released to solution. Nevertheless, the 10:1 ratio in the aqueous Ca and Si concentrations indicated an excess of Ca release relative to pure dicalcium silicate dissolution (i.e. Ca:Si ≈ 2:1) suggesting that free lime was the dominant Ca bearing phase that was dissolving over 24 h.

The difference in the final pH of the 1 and 50 day tests with the same acid addition indicates that part of the alkalinity generation occurs over longer time periods. At high pH this was most likely associated with continued dissolution of dicalcium silicate, although the Si concentrations decreased between day 1 and 50. This Si decrease was most likely associated with the formation of secondary Si-containing phases. These phases were most probably calcium-silicate-hydrate (Ca-Si-H) phases at pH values >9 (Walker et al., 2016; Costa et al., 2016) and amorphous silica ($SiO_{2\ (am)}$) at lower pH values (Langmuir, 1997). The increase in Mg concentration between day 1 and 50 at pH values <9 suggests periclase hydration also continued beyond 24 h.

4.3. Leaching behaviour under aerated conditions

At the initial sampling point (1 h) during the aerated leaching tests, the pH value was 11.5 ± 0.2 and both Ca and Si were released to solution. This rapid initial release of alkalinity, Ca and Si was due

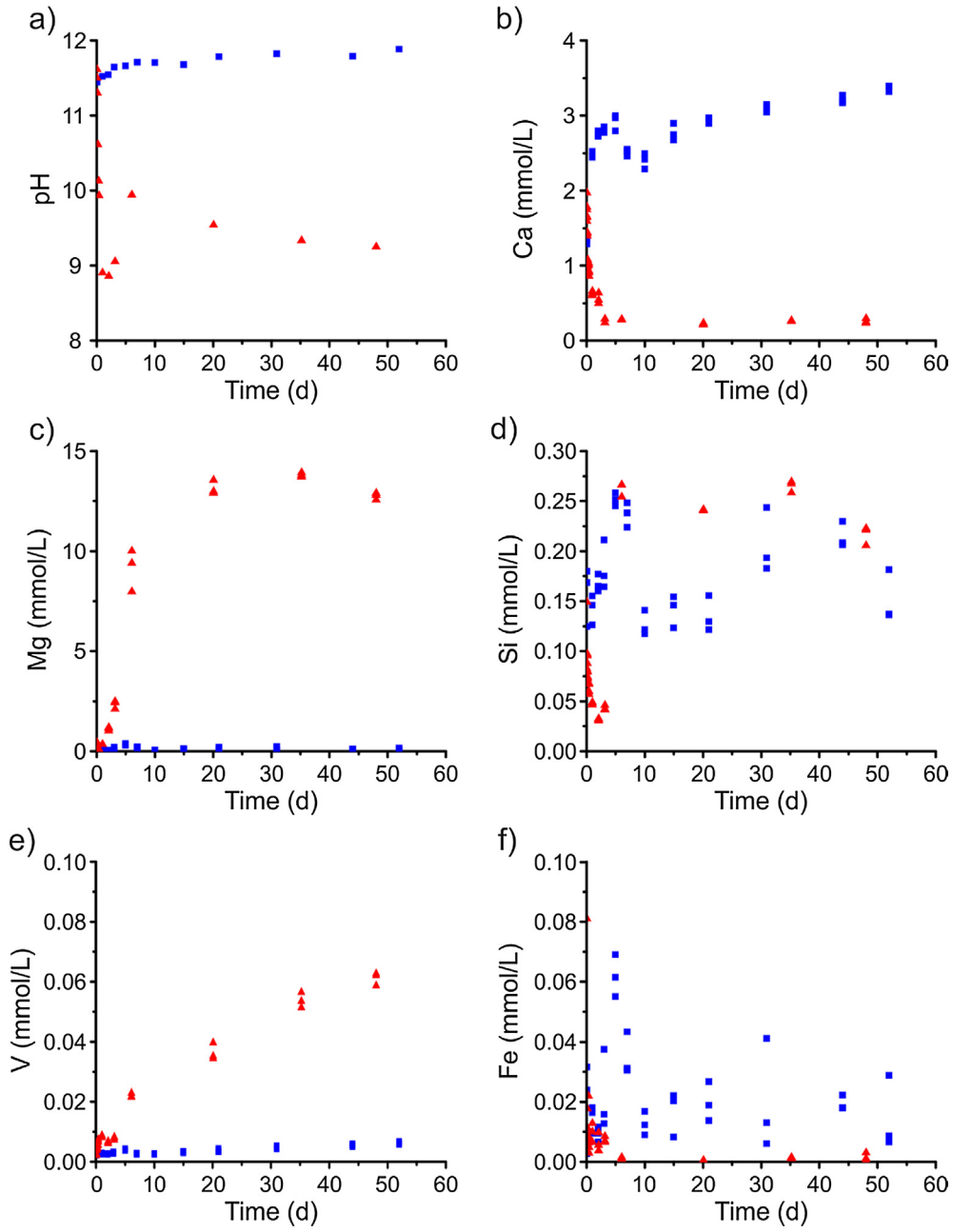

Fig. 4. Leachate composition during the aerated (red triangle) and air-excluded (blue square) batch leaching test on steelmaking waste (initial test conditions: 10 g solid/L deionised water). Data from triplicate experiments shown separately. (For interpretation of the references to colour in this figure legend, the reader is referred to the web version of this article.)

to the hydration and dissolution of both free lime and dicalcium silicate phases present in the waste. Previous slag leaching tests using granulated BOF slag pieces found dicalcium silicate dissolution to be significantly slower than free lime dissolution (Stewart et al., 2018). The use of crushed powder samples in these tests which will have contained high surface area fines must have promoted rapid initial dissolution of dicalcium silicate. However, as dicalcium silicate dissolution releases Ca and Si to solution in an approximately 2:1 ratio (Hobson et al., 2017), the much higher initial Ca/Si ratios in solution (between 13 and 20) indicates that free lime dissolution was most likely to be the predominant source of rapidly leached alkalinity in these tests.

In the 2 days after the initial release of alkalinity Ca and Si to solution, the pH reduced to 8.9 contemporaneously with rapid Ca and Si removal. The decrease in pH and Ca concentrations coincides with the appearance of calcite peaks in the XRD plots after 1 h (Fig. 1) indicating that the initial spike in pH was buffered down to 8.9 due to in-gassing of atmospheric CO_2 and the subsequent precipitation of $CaCO_3$, which consumes both OH^- and Ca^{2+} ions (Eq. (4)). The contemporaneous decrease in Si concentrations may be evidence of the formation of a calcium silicate hydrate phase (Ca-Si-H). Indeed, low Ca/Si ratio (<1) Ca-Si-H phases are predicted to form under the observed initial pH and Ca concentrations on a timescale of 24–48 h (Walker et al., 2016). The peaks associated with dicalcium silicate (larnite) in XRD patterns became less prominent over time and were ultimately absent by the end of the experiments, indicating continued dicalcium silicate dissolution beyond day 6. Despite this no further increase in Ca concentra-

tion was observed after 2 days, probably because most of the Ca released by dicalcium silicate dissolution was precipitated as $CaCO_3$ under aerated conditions (monohydrocalcite peaks became increasingly prominent in the XRD pattern over time). Si concentration increased to a maximum value between 2 and 6 days contemporaneously with a second observed peak in pH. There are only modest changes in Si concentrations observed after 6 days, suggesting that equilibrium with secondary Si-containing phases such as Ca-Si-H or amorphous SiO_2 (Langmuir, 1997, Costa et al., 2016, De Windt et al., 2011) was limiting Si concentrations in these experiments.

XRD analysis indicates that there was progressive loss of periclase from the solids over time, such that it was absent from the final XRD pattern. There were also small brucite peaks in the XRD patterns from all time points. Periclase hydrates in water to form brucite ($Mg(OH)_2$), which readily dissolves at pH values <10.4 (Eq. (2)). No significant Mg release to solution was observed during the first 24 h of leaching because brucite is relatively insoluble at the then prevailing high pH value that was imposed by CaO and calcium silicate weathering. After the initial spike in the pH value on the first day, the solution pH was lower than the brucite equilibrium value, and the aqueous Mg concentration increased as brucite dissolved. As a result, periclase hydration and brucite dissolution provided an additional source of alkalinity to the system. Dissolution of brucite leads to a switch in solution chemistry from a Ca to an Mg dominated system. Monohydrocalcite was observed in XRD patterns after day 6, after which it becomes the dominant carbonate phase, demonstrating a switch from calcite formation in the Mg-free early part of the experiments to predominately monohydrocalcite formation in the Mg-dominated system present after day 6. Recent studies have shown that an Mg-rich environment, such as that observed after 5 days, may support the precipitation of monohydrocalcite ($CaCO_3{\cdot}H_2O$) into which Mg may be incorporated (Rodriguez-Blanco et al., 2014). At later time points dolomite ($CaMg(CO_3)_2$) was detected in XRD analysis, which may also form due to the high Mg concentrations suppressing calcite or aragonite formation during recrystallisation of monohydrocalcite (Rodriguez-Blanco et al., 2014).

4.4. Leaching behaviour under air-excluded conditions

At the first sampling point at 1 hr the pH value and the Ca and Si concentrations were very similar to those observed in the aerated experiments (pH 11.5 ± 0.2, [Ca] 1.5 ± 0.5 mmol L^{-1} and [Si] 0.15 ± 0.025 mmol L^{-1}) indicating similar processes were occurring over the first hour of leaching in both experiments (i.e. rapid dissolution of free lime and fine grained dicalcium silicate particles). As a saturated $Ca(OH)_2$ solution will reach a pH of ~12.5 (Eq. (1)) and experimental pH values were between 11 and 12 at all-time points, it suggests that the magnitude of the initial rise in pH was mass limited (i.e. controlled by the amounts of CaO and reactive dicalcium silicate that are readily available for dissolution) rather than $Ca(OH)_2$ solubility limited. Between the first sampling point and day 5 there was a slow increase in pH, Ca and Si which was probably the result of continued dicalcium silicate dissolution.

Between day 5 and 10 in the air-excluded experiments there was a decrease in Ca concentrations that coincided with a decrease in Si concentrations, which suggests that a Ca-Si-H phase formed. The pH, Ca and Si concentrations present at the time of formation in the leaching experiments were consistent with precipitation of a Ca-Si-H phase with Ca/Si ratio of close to 1 (Walker et al., 2016). The continuing slow rise in pH, Ca and Si concentrations during the remainder of the experiment indicate that under air-excluded conditions, the solution composition slowly evolves towards dicalcium silicate solubility limits over time (also observed by De Windt et al., 2011). However, Ca-Si-H gel formation can cover particle surfaces, making alkalinity generation a diffusion-limited process (Hobson et al., 2017; Costa et al., 2016; Nikolić et al., 2016), slowing the dissolution of the remaining reactive solid phases, and leading to the incomplete dissolution of larnite (dicalcium silicate) observed at the end of these experiments (Fig. 1b). No Mg was released to solution under air-excluded conditions because the pH remained above 10.4 throughout the experiments, and therefore, dissolution of the Mg containing phases was inhibited.

4.5. Control of trace metal release

Fe can be released to solution during dissolution of both free lime and dicalcium silicate (in which it can be a minor constituent; Hobson et al., 2017), and therefore Fe is present in the leachate throughout the air-excluded experiments (The slightly lower Fe concentrations after 5 days under air-excluded conditions may be due in part to incorporation of some Fe into Ca-Si-H phases). Conversely, under aerated conditions Fe is only present in significant concentrations during the first 3 days during which time the leachate pH falls from 11.5 to 9. Under aerated conditions, any Fe(II) released is likely to be readily oxidised to Fe(III) and precipitated either as an insoluble hydroxide or incorporated into spinel-like secondary phases (e.g. magnetite, Fe_3O_4: De Windt et al. (2011)) at pH 9, limiting Fe accumulation in solution.

Vanadium release in the air-excluded experiments is low (maximum of ~0.007 mmol L^{-1}) compared to that observed in the aerated experiments (maximum of ~0.065 mmol L^{-1}). Previous work on BOF slag weathering suggests that it is V(V) associated with dicalcium silicate which is most readily leached to solution (Hobson et al., 2017), which is present in high pH solution as the vanadate oxyanion (VO_4^{3-}; Wehrli and Stumm, 1989). Thus, V concentrations observed during BOF slag leaching are likely to be controlled by $Ca_3(VO_4)_2$ solubility limits ($K_{sp} = 10^{-17.97}$; Huijgen and Comans, 2006; Cornelis et al., 2008; Allison et al., 1991) which impose an inverse relationship between Ca and V concentrations in the leachate (Fig. 5).

$$3Ca^{2+} + 2VO_4{}^{3-} \rightleftharpoons Ca_3(VO_4)_2 \quad (6)$$

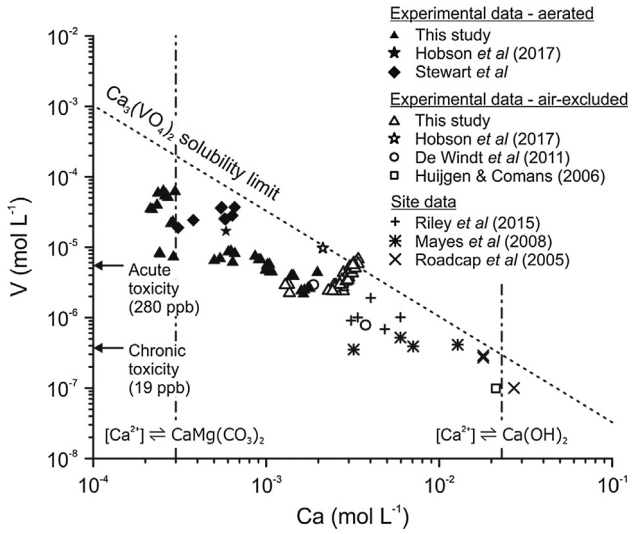

Fig. 5. Plot of [V] versus [Ca] for selected experimental and site data (site data from Riley and Mayes, 2015; Roadcap et al., 2005; Mayes et al., 2008). The dashed line marks the solubility limits for $Ca_3(VO_4)_2$ at 20 °C (Allison et al., 1991). Data plotting below the solubility limit is undersaturated with respect to that phase. Vertical dashed lines indicate [Ca] in solutions in equilibrium with dolomite in contact with atmospheric CO_2, or with $Ca(OH)_2$, respectively (both at 20 °C). Horizontal arrows indicate acute and chronic freshwater toxicity guideline limits (Buchman, 2008) (figure redrawn after Hobson et al., 2017).

Under air-excluded conditions Ca released from CaO and dicalcium silicate weathering accumulated in solution, producing a leachate with high Ca concentrations. The leachate solution, therefore, quickly reached $Ca_3(VO_4)_2$ solubility limits, preventing further release of V to solution and limiting V concentrations in the leachate.

Aerated conditions, however, allow in-gassing of atmospheric CO_2 and associated formation of secondary carbonate minerals. This process provides a sink for Ca, lowering aqueous Ca concentrations. The V that is released therefore persists in solution (due to the lower $[Ca^{2+}]\cdot[VO_4^{3-}]$ ion activity product), leading to much higher concentrations than those seen under air-excluded conditions. Monohydrocalcite is relatively soluble ($Ksp = 1 \times 10^{-7.1}$; Kralj and Brečević, 1995), therefore, the equilibrium phase controlling Ca concentrations in these experiments is probably dolomite ($CaMg(CO_3)_2$; $Ksp = 1 \times 10^{-17.2}$; Sherman and Barak, 2000). Indeed, the predicted Ca concentration in solutions equilibrated with dolomite and atmospheric pCO_2 are similar to those found at the end of these experiments (Fig. 5; Langmuir, 1997). In the aerated experiments, the overall leachate chemistry remains undersaturated with respect to $Ca_3(VO_4)_2$, which is consistent with the observed depletion of the V-hosting dicalcium silicate phase by the end of the aerated experiments.

4.6. Implications for waste management

Co-disposed wastes such as those used in this study are unattractive for reuse in furnaces due to their highly variable composition making it difficult to control the steelmaking processes. Furthermore, the presence of MgO makes their reuse in civil engineering applications difficult, since periclase hydration to form brucite leads to significant volumetric expansion and cracking. Given these problematic characteristics, combined steelmaking wastes are generally stored in landfill. Over time, rainwater inevitably infiltrates and reacts with landfilled waste to generate leachate. Therefore, the storage environment plays a key role in establishing leachate composition. There is a key interaction between Ca concentrations and the solution pH, which controlled by the equilibrium with the dominant Ca-phase present (i.e. portlandite, Ca-Si-H or $CaCO_3$). The presence of CO_2 is a key factor in determining which secondary Ca phases are present during leaching and also the degree to which the primary dicalcium silicate was leached (therefore, indirectly affecting the release of trace metals such as V).

Under air-excluded conditions, the leaching profile of the combined waste is similar to that of BOF slag (Hobson et al., 2017; De Windt et al., 2011; Huijgen and Comans, 2006; Costa et al., 2016). Rapid dissolution of Ca-bearing phases without in-gassing of CO_2 leads to a high pH, $Ca(OH)_2$ dominated leachate. High Ca concentrations limit V release due to $Ca_3(VO_4)_2$ solubility limits. Consequently, water saturated environments with limited opportunity for CO_2 ingress will provide the safest environment for waste storage. Leachate could either be recirculated (and reach equilibrium with $Ca(OH)_2$) or be removed and treated off site to lower its pH and allow carbonation without triggering V release (Gomes et al., 2017). Under aerated conditions, lower alkalinity and Ca concentrations allow much higher V concentrations to accumulate in leachate, as well as allowing dissolution of MgO to form a $Mg(OH)_2$ dominated leachate which favours the formation of monohydrocalcite and dolomite as secondary carbonate phases. Leaching under aerated conditions rapidly produces leachate with V concentrations in excess of acute toxicity thresholds (280 $\mu g\,L^{-1}$; Fig. 5) and all experiments display V concentrations higher than chronic toxicity thresholds (19 $\mu g\,L^{-1}$, Buchman, 2008). New proposals for V exposure based on recent reviews of ecotoxicology data (Smit, 2012) have suggested new water quality standards for V of 1.2 and 3.0 $\mu g\,L^{-1}$ for chronic and acute exposure respectively. Almost all slag leachates reported (Fig. 5) would exceed these more stringent limits, therefore, leachate generated from co-disposed steel making wastes would require careful management (and treatment prior to discharge) to avoid the potential for environmental harm.

Extrapolating from experimental results to field scale predictions must always be done with caution. For example, these experiments were performed on crushed powder samples at much lower solid to liquid ratios than would typically be found in a heap leaching scenario. It is much more likely that during heap leaching (due to high solid:solution ratios present) free lime and dicalcium silicate dissolution will control leachate quality resulting in higher Ca concentrations (i.e. leachate saturated with respect to Ca $(OH)_2$) and therefore lower V concentrations compared to those seen in experimental systems (indeed most real site leachates commonly contain V at order of magnitude lower concentrations than found in laboratory experiments; Fig. 5). However, the experimental results indicate that although carbonation reactions are helpful in reducing pH and alkalinity over time, the lower Ca concentrations produced may allow higher V concentrations to accumulate in leachates over time. Therefore leachates produced from co-disposed steelmaking wastes will likely require monitoring and secondary treatments (e.g. by employing wetlands or cascade systems; Gomes et al., 2017) for decades after their initial disposal.

5. Conclusions

The co-disposed waste investigated in this study was composed of BOF steelmaking slag containing dicalcium silicate, wüstite, dicalcium aluminoferrite and free lime; and refractory oxides comprising corundum, periclase, graphite and high temperature aluminosilicate. V was predominately associated with the dicalcium silicate and dicalcium aluminoferrite phases. During leaching, alkalinity was produced by dissolution of free lime and dicalcium silicate. Under air-excluded conditions high Ca concentrations and the inverse relationship between Ca and V concentrations imposed by $Ca_3(VO_4)_2$ solubility limits restricted V release to the leachate. Under aerated conditions in-gassing of CO_2 promoted carbonation reactions and secondary carbonate formation. Leachate pH and Ca concentrations were reduced and MgO hydration and dissolution was promoted leading to a switch from a Ca to an Mg dominated leachate and precipitation of monohydrocalcite and dolomite. V concentrations in leachate were higher under aerated conditions where formation of carbonate minerals provides a sink for aqueous Ca following in-gassing of CO_2. Under these conditions, the inverse relationship imposed by $Ca_3(VO_4)_2$ solubility limits allows higher concentrations of V to accumulate in leachate than those seen under air-excluded conditions. Therefore, when considering long-term leaching behaviour, it is important that risk assessments consider the expected *in situ* environmental chemistry of specific waste storage environments.

Acknowledgements

This research was funded by a UK Natural Environment Research Council PhD studentship to AJH and UK NERC grants NE/L01405X/1 and NE/L014211/1 under the Resource Recovery from Waste theme. We thank Andy Connelly, Lesley Neve, Stephen Reid, Richard Walshaw and Duncan Hedges (all University of Leeds) for lab assistance, XRD, ICP-OES/MS and SEM analysis respectively. We also thank Nick Marsh at the University of Leicester and Bob Knight at the University of Hull for XRF and additional ICP-OES respectively.

References

Allison, J.D., Brown, D.S., Novo-Gradac, K.J., 1991. MINTEQA2/PRODEFA2, a Geochemical Assessment Model for Environmental Systems: Version 3.0 User's Manual. Environmental Research Laboratory, Office of Research and Development, US Environmental Protection Agency.

Bayless, E.R., Schulz, M.S., 2003. Mineral precipitation and dissolution at two slag-disposal sites in northwestern Indiana, USA. Environ. Geol. 45, 252–261.

Buchman, M.F., 2008. NOAA Screening Quick Reference Tables. Office of Response and Restoration Division, National Oceanic andAtmospheric Administration, Washington, DC.

Chaurand, P., Rose, J., Domas, J., Bottero, J.Y., 2006. Speciation of Cr and V within BOF steel slag reused in road constructions. J. Geochem. Explor. 88, 10–14.

Chesters, J.H., 1973. Refractories: Production and Properties. Iron and Steel Institute.

Cornelis, G., Johnson, C.A., Gerven, T.V., Vandecasteele, C., 2008. Leaching mechanisms of oxyanionic metalloid and metal species in alkaline solid wastes: a review. Appl. Geochem. 23, 955–976.

Costa, G., Polettini, A., Pomi, R., Stramazzo, A., 2016. Leaching modelling of slurry-phase carbonated steel slag. J. Hazard. Mater. 302, 415–425.

Dana, K., Das, S.K., 2004. Partial substitution of feldspar by B.F. slag in triaxial porcelain: phase and microstructural evolution. J. Eur. Ceram. Soc. 24, 3833–3839.

de Sa, R.G., e Silva, G.L., Bitttencourt, L., 2007. Recycling of spent refractories from metallurgical processing management and technological approach. 8th UNITECR, Dresden, Alemania.

de Windt, L., Chaurand, P., Rose, J., 2011. Kinetics of steel slag leaching: Batch tests and modeling. Waste Manage. 31, 225–235.

Eloneva, S., Puheloinen, E.-M., Kanerva, J., Ekroos, A., Zevenhoven, R., Fogelholm, C.-J., 2010. Co-utilisation of CO_2 and steelmaking slags for production of pure $CaCO_3$ – legislative issues. J. Cleaner Prod. 18, 1833–1839.

ENVIRONMENT AGENCY 2014. EA Bespoke permit 2014 Permit for Scunthorpe Aggregate processing. Permit number EPR/LP3537VV/A001.

Geiseler, J., 1996. Use of steelworks slag in Europe. Waste Manage. 16, 59–63.

Gomes, H.I., Rogerson, M., Burke, I.T., Stewart, D.I., Mayes, W.M., 2017. Hydraulic and biotic impacts on neutralisation of high-pH waters. Sci. Total Environ. 601–602, 1271–1279.

Hanagiri, S., Matsui, T., Shimpo, A., Aso, S., Inuzuka, T., Matsuda, T., Sakaki, S., Nakagawa, H., 2008. Recent improvement of recycling technology for refractories. SHINNITTETSU GIHO 388, 93.

Hobson, A.J., Stewart, D.I., Bray, A.W., Mortimer, R.J.G., Mayes, W.M., Rogerson, M., Burke, I.T., 2017. Mechanism of vanadium leaching during surface weathering of basic oxygen furnace steel slag blocks: a microfocus X-ray absorption spectroscopy and electron microscopy study. Environ. Sci. Technol. 51, 7823–7830.

Huijgen, W.J.J., Comans, R.N.J., 2006. Carbonation of steel slag for CO_2 sequestration: leaching of products and reaction mechanisms. Environ. Sci. Technol. 40, 2790–2796.

Kralj, D., Brečević, L., 1995. Dissolution kinetics and solubility of calcium carbonate monohydrate. Colloids Surf. A: Physicochem. Eng. Aspects 96, 287–293.

Kwong, K., Bennett, J., 2002. Recycling practices of spent MgO-C refractories. J. Miner. Mater. Charact. Eng. 1, 69–78.

Langmuir, D., 1997. Aqueous Environmental Geochemistry. Prentice Hall.

Matern, K., Rennert, T., Mansfeldt, T., 2013. Molybdate adsorption from steel slag eluates by subsoils. Chemosphere 93, 2108–2115.

Mayes, W.M., Younger, P.L., 2006. Buffering of alkaline steel slag leachate across a natural wetland. Environ. Sci. Technol. 40, 1237–1243.

Mayes, W.M., Younger, P.L., Aumonier, J., 2008. Hydrogeochemistry of alkaline steel slag leachates in the UK. Water Air Soil Pollut. 195, 35–50.

Mazdiyasni, K.S., Brown, L.M., 1972. Synthesis and mechanical properties of stoichiometric aluminum silicate (Mullite). J. Am. Ceram. Soc. 55, 548–552.

Navarro, C., Diaz, M., Villa-Garcia, M.A., 2010. Physico-chemical characterization of steel slag. Study of its behavior under simulated environmental conditions. Environ. Sci. Technol. 44, 5383–5388.

Nikolić, I., Drinčić, A., Djurović, D., Karanović, L., Radmilović, V.V., Radmilović, V.R., 2016. Kinetics of electric arc furnace slag leaching in alkaline solutions. Construct. Build. Mater. 108, 1–9.

Ober, J.A., 2017. Mineral commodity summaries 2017. Mineral Commodity Summaries. Reston, VA.

Piatak, N.M., Parsons, M.B., Seal, R.R., 2014. Characteristics and environmental aspects of slag: a review. Appl. Geochem.

Pourbaix, M., 1966. Atlas of Electrochemical Equilibria in Aqueous Solutions. Pergamon Press.

Proctor, D.M., Fehling, K.A., Shay, E.C., Wittenborn, J.L., Green, J.J., Avent, C., Bigham, R.D., Connolly, M., Lee, B., Shepker, T.O., Zak, M.A., 2000. Physical and chemical characteristics of blast furnace, basic oxygen furnace, and electric arc furnace steel industry slags. Environ. Sci. Technol. 34, 1576–1582.

Quaranta, N.E., Caligaris, M.G., Díaz, O., 2014. Characterization of converter refractories for recycling. In: Materials Science Forum. Trans Tech Publ, pp. 605–610.

Riley, A.L., Mayes, W.M., 2015. Long-term evolution of highly alkaline steel slag drainage waters. Environ. Monit. Assess. 187, 463.

Roadcap, G.S., Kelly, W.R., Bethke, C.M., 2005. Geochemistry of extremely alkaline (pH > 12) ground water in slag-fill aquifers. Ground Water 43, 806–816.

Rodriguez-Blanco, J.D., Shaw, S., Bots, P., Roncal-Herrero, T., Benning, L.G., 2014. The role of Mg in the crystallization of monohydrocalcite. Geochim. Cosmochim. Acta 127, 204–220.

Rovnushkin, V.A., Visloguzova, E.A., Spirin, S.A., Shekhovtsov, E.V., Kromm, V.V., Metelkin, A.A., 2005. Composition of ladle slag and refractory materials and its effect on the wear resistance of the lining of an RH vacuum degasser. Refractories Ind. Ceram. 46, 193–196.

Schneider, H., Okada, K., Pask, J.A., 1994. Mullite and Mullite Ceramics. J. Wiley.

Sherman, L.A., Barak, P., 2000. Solubility and dissolution kinetics of dolomite in Ca–Mg–HCO_3/CO_3 solutions at 25°C and 0.1 MPa carbon dioxide. Soil Sci. Soc. Am. J. 64, 1959–1968.

Shi, C., 2002. Characteristics and cementitious properties of ladle slag fines from steel production. Cem. Concr. Res. 32, 459–462.

Shi, H., Zhao, Y., Li, W., 2002. Effects of temperature on the hydration characteristics of free lime. Cem. Concr. Res. 32, 789–793.

Smit, C.E., 2012. Environmental Risk Limits for Vanadium in Water: A Proposal for Water Quality Standards in Accordance with the Water Framework Directive. RIVM Letter Report 601714021/2012. National Institute for Public Health and the Environment.

Stewart, D.I., Bray, A.W., Udoma, G., Hobson, A.J., Mayes, W.M., Rogerson, M., Burke, I.T., 2018. Hydration of dicalcium silicate and diffusion through neo-formed calcium-silicate-hydrates at weathered surfaces control the long-term leaching behaviour of basic oxygen furnace (BOF) steelmaking slag. Environ. Sci. Pollut. Res. 25, 9861–9872.

Tamari, N., Kondoh, I., Tanaka, T., Katsuki, H., 1993. Mechanical properties of alumina-mullite whisker composites. J. Ceram. Soc. Jpn. 101, 721–724.

Taylor, H.F.W., 1986. Proposed structure for calcium silicate hydrate gel. J. Am. Ceram. Soc. 69, 464–467.

Tossavainen, M., Engstrom, F., Yang, Q., Menad, N., Lidstrom Larsson, M., Bjorkman, B., 2007. Characteristics of steel slag under different cooling conditions. Waste Manage. 27, 1335–1344.

Walker, C.S., Sutou, S., Oda, C., Mihara, M., Honda, A., 2016. Calcium silicate hydrate (C-S-H) gel solubility data and a discrete solid phase model at 25°C based on two binary non-ideal solid solutions. Cem. Concr. Res. 79, 1–30.

Wehrli, B., Stumm, W., 1989. Vanadyl in natural-waters – adsorption and hydrolysis promote oxygenation. Geochim. Cosmochim. Acta 53, 69–77.

Yi, H., Xu, G., Cheng, H., Wang, J., Wan, Y., Chen, H., 2012. An overview of utilization of steel slag. Proc. Environ. Sci. 16, 791–801.

Yildirim, I.Z., Prezzi, M., 2011. Chemical, mineralogical, and morphological properties of steel slag. Adv. Civ. Eng. 2011, 1–13.

Zhao, L., Li, Y., Zhou, Y., Cang, D., 2014. Preparation of novel ceramics with high CaO content from steel slag. Mater. Des. 64, 608–613.